Analyst

ROYAL SOCIETY OF CHEMISTRY

PAPER

View Article Online
View Journal

Cite this: DOI: 10.1039/d0an01204a

Selective detection of phospholipids in human blood plasma and single cells for cancer differentiation using dispersed solid-phase microextraction combined with extractive electrospray ionization mass spectrometry†

Hua Zhang,[a,b] Haiyan Lu,[b] Keke Huang,[b] Jiajia Li,[c] Feng Wei,[d] Aiying Liu,[b] Konstantin Chingin*[a] and Huanwen Chen*[a,b]

Phospholipids in microvolume biofluid samples (≤0.5 μL), including human plasma and single cells, were selectively captured by dispersed magnetic Fe_3O_4@TiO_2 nanocomposite particles (40 μg). A suspension containing Fe_3O_4@TiO_2 nanoparticles was loaded into a glass capillary (i.d. 0.75 mm) by capillary force. The supernatant solution was discarded, while the Fe_3O_4@TiO_2 particles were retained inside the capillary by using an external magnetic field (*ca.* 1.3 T). The phospholipids on the surface of Fe_3O_4@TiO_2 nanoparticles were directly analyzed using internal extractive electrospray ionization mass spectrometry (iEESI-MS) by pumping ≤1 μL of extraction solution of methanol containing 1.5% ammonia (w/w) through the capillary tube toward the ESI tip. A single sample analysis was accomplished within 4 min. Phospholipids in blood plasma samples from 59 patients with ovarian cancer and 43 healthy controls, and 28 patients with pancreatic cancer and 23 healthy controls were studied. Based on the orthogonal partial least squares discriminant analysis (OPLS-DA), the cancer patients were confidently discriminated from the healthy controls. Phospholipids in single human cells (MV4–11 and NB4) were determined, showing the sensitivity for single cell analysis. Therefore the results demonstrated that rapid cancer differentiation is achieved using this approach through the detection of trace phospholipids in microvolume blood and cell samples with high sensitivity, high specificity, low sample consumption, and high throughput.

Received 16th June 2020,
Accepted 13th August 2020

DOI: 10.1039/d0an01204a

rsc.li/analyst

1. Introduction

Phospholipids carry out various biological functions in living organisms including formation of membrane structure, chemical-energy storage, protein synthesis, cellular signaling, *etc.*[1–5] Phospholipid composition in cells or tissues can be characteristic of metabolic states. Strong proofs have been established that the metabolism dysregulation of phospholipids is associated with a variety of human diseases such as cancer,[6–8] diabetes,[5,9] Alzheimer's disease,[10–12] and cardiovascular diseases.[13,14] Importantly, chemical profiling of cancer cells at the single-cell level provides helpful data to improve our current understanding of the cell-to-cell heterogeneity and fundamental mechanism of disease.[15–19] Thus, rapid determination of phospholipids in biofluid samples is of significant interest in life science. For example, phospholipid biomarkers for some diseases are highly expected based on the results of earlier studies.[3,20] Studies also showed that the phospholipid components of different types of cells are highly specific.[18,19,21] Analytical technologies including nuclear magnetic resonance spectrometry (NMR),[22,23] infrared spectrometry (IR),[24,25] Raman spectroscopy,[26,27] and mass spectrometry (MS)[6,28] have been applied in the study of phospholipids in biofluid samples. The advantages of MS for phospholipid analysis are its excellent sensitivity and specificity.[6,29,30] Usually, in view of the high complexity of biological matrices, tedious and laborious sample separation processes, such as liquid–liquid extraction, solid phase extraction, thin-layer chromatography (TLC), electrophoresis, capillary electrophor-

[a]*Jiangxi Key Laboratory for Mass Spectrometry and Instrumentation, East China University of Technology, Nanchang 330013, P. R. China.*
E-mail: chingin.k@gmail.com, chw8868@gmail.com
[b]*State Key Laboratory of Inorganic Synthesis and Preparative Chemistry, College of Chemistry, Jilin University, Changchun 130012, P. R. China*
[c]*Department of Obstetrics and Gynecology, The First Hospital of Jilin University, 130021, P. R. China*
[d]*Department of Hepatobiliary and Pancreatic Surgery, The First Hospital of Jilin University, 130021, P. R. China*

†Electronic supplementary information (ESI) available. See DOI: 10.1039/d0an01204a

esis (CE), gas chromatography (GC), (ultra)high-performance liquid chromatography ((U)HPLC) or (ultrahigh-performance) supercritical fluid chromatography ((UHP)SFC), are required before the MS analysis of phospholipids.[3,28,31–33] Separation processes enable high quality of chemical analysis, but unfortunately, require longer time for analysis. Thus, there is a demand for methods that could allow rapid determination of phospholipids in biofluid samples.

Solid-phase microextraction (SPME) is a facile and versatile sample preparation method that has been demonstrated to be efficient for the study of a broad range of complex samples coupled with GC-MS and HPLC-MS.[34–36] Recently, coupling SPME with ambient mass spectrometry (AMS) has provided the opportunity to rapidly enrich the target analytes from complex matrices for direct MS screening without GC/LC chromatography separation, which further improved the analytical throughput.[37,38] Recently, novel SPME based ambient ionization methods have been developed for the rapid determination of trace analytes in complex samples, including coated blade spray,[39] solid-phase microextraction–transmission mode direct analysis of real time,[40] surface-coated probe nanoelectrospray ionization,[41] coated paper spray,[42] TiO_2 nanowire array based internal extractive electrospray ionization,[43] covalent organic framework (COF) based SPME with constant flow desorption ionization,[44] tungsten needle based SPME-probe ESI,[45] fiber based SPME-thermal desorption-electrospray ionization,[46] *etc.* In previous studies, SPME substrates used for AMS include fiber,[41,46] tungsten wire,[45] glass capillary,[47] paper,[42] stainless blade,[39] *etc.* A promising approach to improve the extraction efficiency of conventional fiber-based SPME is dispersed solid-phase microextraction (d-SPME), which is a dispersed mode extraction based on nanoparticles (NPs).[34,48] In d-SPME, functionalized nanoparticles are directly dispersed into the sample matrix for the capture of target analytes. The use of nanoparticles for SPME greatly increases the total active surface area of an adsorbent.[34,48] Unfortunately, cumbersome procedures are typically required in d-SPME for the collection of nanoparticles (after adsorption of the target analytes) as well as for desorption of analytes (in an elution solvent). These procedures are usually based on centrifugation or filtration which requires substantial time. Therefore, the combination of d-SPME and ambient MS for direct chemical analysis presents a considerable challenge.

Internal extractive electrospray ionization (iEESI) is an ambient ionization technique that was developed for the direct analysis of internal chemicals in bulk samples such as plant/animal tissue samples without any sample pretreatments.[49–52] Recently, through coupling with various functional nanomaterials, iEESI-MS approaches have been developed for the targeted determination of trace analytes in complex fluid samples such as human urine,[53,54] human blood,[43] raw milk[55] and environmental water.[56] Herein, a novel d-SPME approach coupled with internal extractive electrospray ionization mass spectrometry (d-SPME–iEESI-MS) was proposed for the rapid determination of phospholipids in microvolume biofluid samples. Extraction and desorption of phospholipids based on Fe_3O_4@TiO_2 nanocomposites were accomplished inside a glass capillary, and the solution containing extracted phospholipids was directly transferred to a connected electrospray emitter for MS analysis. It is well established that titanium oxide (TiO_2) can reversibly bind with phosphate group-containing compounds, such as phosphopeptides,[57] phospholipids,[58] and organophosphorus pesticides,[59] with high specificity. In this study, magnetic Fe_3O_4@TiO_2 nanocomposites were synthesized for the enrichment of phospholipids from microvolume biofluid samples using d-SPME coupled with iEESI-MS. The magnetic Fe_3O_4@TiO_2 nanocomposites allow rapid isolation of phospholipids from the sample matrix using an external magnetic field without any centrifugation or filtration. The proposed approach was successfully applied to differentiate the blood plasma samples from ovarian cancer patients, pancreatic cancer patients, and healthy volunteers, as well as to detect phospholipids in single human cells (MV4–11 and NB4).

2. Experimental section

2.1 Materials and chemicals

Biofluid samples involved in this study include human blood plasma and cancer cells. Human blood plasma samples from ovarian cancer patients, pancreatic cancer patients, and healthy volunteers were provided by The First Hospital of Jilin University (Changchun, China), with full consent from all the volunteers. A total of 102 human blood plasma samples containing 59 samples from ovarian cancer patients and 43 samples from healthy volunteers as the control group and a total of 51 blood plasma samples containing 28 samples from pancreatic cancer patients and 23 samples from healthy volunteers were used in this study (for details see Table S1, ESI†). The samples included in this study were chosen based on the results of the histopathological analysis of the patients. Cell lines (MV4–11 and NB4) were purchased from American Type Culture Collection, and were cultured in RPMI 1640 containing 10% fetal bovine serum (FBS) (Life Technology). Note that the experiments of human blood plasma and cancer cells were adhered to the tenets of Helsinki Declaration,[60] and approved by the Ethics Committee of the Jilin University and The First Hospital of Jilin University. For details about the materials and chemicals used in the study, refer to the ESI.†

2.2 Preparation of Fe_3O_4@TiO_2 magnetite nanocomposites

Fe_3O_4@TiO_2 magnetic nanocomposites were synthesized using a hydrothermal method and the sol–gel process. Fe_3O_4 magnetic nanoparticles were firstly synthesized using a hydrothermal method and then the obtained Fe_3O_4 nanoparticles were coated with TiO_2 by the sol–gel process. For details about the preparation and characterization of Fe_3O_4@TiO_2 magnetic nanocomposites, refer to the ESI.†

2.3 Sampling method

The schematic analytical workflow of d-SPME–iEESI-MS is shown in Fig. 1. Selective extraction of phospholipids from

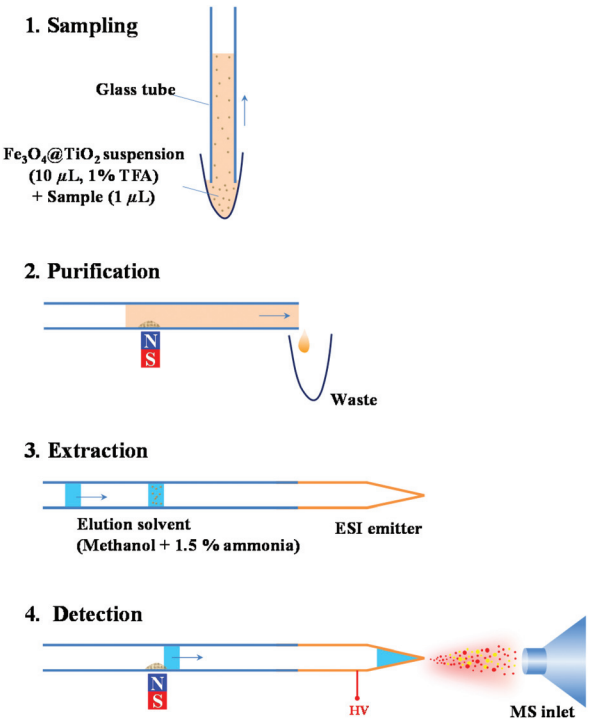

Fig. 1 Schematic illustration of d-SPME–iEESI-MS analysis.

biological samples was achieved using Fe_3O_4@TiO_2 nanocomposites within a glass capillary tube for direct iEESI-MS analysis. Briefly, an aliquot of 0.5 μL of sample and 10 μL of Fe_3O_4@TiO_2 nanocomposite water suspension (corresponding to 40 μg of Fe_3O_4@TiO_2 nanocomposite material) were mixed in a 0.2 mL Eppendorf tube. Note that 1% TFA was added to the water suspension of Fe_3O_4@TiO_2 before use. The mixture was pipetted back and forth for homogeneous mixing. Then, the sample solution was loaded into the glass capillary tube (i.d. 0.75 mm, o.d. 1 mm, and length 100 mm, borosilicate glass) by capillary force. For purification of the sample, the Fe_3O_4@TiO_2 nanocomposite material was magnetically collected and retained inside of the capillary tube by using an external magnetic field (*ca.* 1.3 T), while the supernatant was discarded. In this way, the Fe_3O_4@TiO_2 nanocomposites with the adsorbed phospholipids were separated from the sample matrix solution. After the sample matrix solution was discarded, the Fe_3O_4@TiO_2 nanocomposites inside the capillary were flushed with 1 μL of methanol containing1.5% NH_4OH to desorb the phospholipids from the Fe_3O_4@TiO_2 nanocomposites. This step required ≤10 s. After that, the extraction solution was pumped forward along the capillary toward the silver-coated ESI tip by air pressure. Meanwhile, the Fe_3O_4@TiO_2 nanocomposite material was retained in the glass capillary by using an magnetic field (~1.3 T). The ESI tip was placed horizontally pointing toward the MS ion inlet at a distance of 4 mm away from the MS ion inlet. A high voltage of +4.0 kV was applied to the ESI tip to generate electrospray plume.

2.4 Single-cell sampling

Single-cell samples were prepared through the serial dilution method according to the previous literature.[61,62] Briefly, MV4–11 and NB4 cells were trypsinized by Trypsin-EDTA (0.25%) to obtain fresh cell suspensions prior to MS analysis. The cell suspensions were subsequently dispersed into PBS solution. Then, centrifugation (1000 rpm, 5 min) was performed to remove the residual culture medium in the cell solution, and the cells were resuspended into PBS solution at a density of *ca.* 1×10^6 cells per mL. The cell concentration was determined using a hemocytometer. The cell suspension was further diluted to a density of *ca.* 2×10^3 cells per mL using PBS. The cell suspension was magnetically stirred during the experiment using a magnetic stick (100 rpm) in order to prevent cell aggregation and cell sinking. Each 0.5 μL aliquot of the diluted cell suspension was loaded into the corresponding well of a 96-well microtiter plate, and the number of cells within the sample spot was calculated using a microscope (TI-S, NIKON, Japan). Theoretically, the probability of single-cell distribution in one sample spot follows random dispersion (Fig. S1, ESI†). Only the samples with single-cell distribution were used for d-SPME–iEESI-MS analysis. Similar to the analysis of human blood plasma samples, a slightly modified handling procedure was used for the analysis of single-cell samples. For better sensitivity of detection, 10 μL of methanol suspension of Fe_3O_4@TiO_2 nanocomposite containing 1% TFA was mixed with 0.5 μL of single-cell suspension sample for the extraction of phospholipids. The mixture was pipetted back and forth for an efficient extraction. The volume of the elution solution was decreased to 0.5 μL. Note that the cells are readily decomposed under the non-isosmotic environment, and the phospholipids released from the cell become available for adsorption by Fe_3O_4@TiO_2 nanoparticles.

2.5 Mass spectrometry

The experiments were carried out using an Orbitrap Fusion™ Tribrid™ mass spectrometer (Thermo Scientific, San Jose, CA, USA). Mass spectra were obtained in the mass range *m*/*z* 300–1000 under positive ion detection mode. The heated ion capillary was maintained at 320 °C. For MS/MS analysis, higher-energy collisional dissociation (HCD) experiments were carried out with precursor ions isolated using a window width of 1.0 Da, and normalized collision energy (NCE) was set to 20–40%. Other parameters were set to default instrument values without any further optimization.

2.6. Chemical identification and data analysis

Chemical assignment was based on high resolution MS data, HCD experiments, authentic compounds, and earlier literature reports,[3,6,63,64] as well as searching the Human Metabolome Database (http://www.hmdb.ca). The statistical method of orthogonal partial least squares discriminant analysis (OPLS-DA) was used to process the mass fingerprints collected from different types of patients according to previous studies.[65,66] Briefly, the mass spectral data were exported into

Microsoft Excel and arranged with the *m/z* values as independent variables, in which the *m/z* value and its signal intensity exported from each sample case were matched, respectively. The exported data in Excel were aligned based on the *m/z* value of each sample case using Matlab (Version 7.8.0, Mathworks, Inc., Natick, MA) prior to OPLS-DA analysis using SIMCA (Version 14.1, Umetrics, Sweden). Furthermore, Q^2 and R^2 parameters were determined and 200 permutation tests were performed to confirm the robustness, predictive power, and validity of the OPLS-DA model.

3. Results and discussion

3.1 d-SPME–iEESI-MS

The synthesized Fe_3O_4@TiO_2 nanocomposites were characterized using SEM, EDX, TEM, and XRD (Fig. S2, ESI†). The characterization results confirm the coating of TiO_2 on the Fe_3O_4 nanoparticles. The Fe_3O_4@TiO_2 nanocomposites were spherical in shape with a size of *circa* 300 nm. Both the EDX and XRD results indicate that TiO_2 on the surface belong to the anatase phase (JCPDS file No. 84-1286).

In d-SPME–iEESI-MS, phospholipids are adsorbed on the surface of Fe_3O_4@TiO_2 nanocomposites at acidic pH and readily released at alkaline pH. The retention of phospholipids on the surface of Fe_3O_4@TiO_2 nanocomposites is based on the Lewis acid–base interactions. The phosphate moiety of phospholipids, being a Lewis base, interacts with the empty d-orbitals of the transition metal, which acts as a Lewis acid at acidic pH.[67–69] Desorption of phospholipids from the Fe_3O_4@TiO_2 nanocomposites is achieved at alkaline pH. Thus, the suspension of Fe_3O_4@TiO_2 nanocomposites (40 μg) in water (10 μL) was acidified with 1% TFA to pH = 1 prior to the d-SPME process. Deproteinization of blood plasma was not found to take place during the extraction of phospholipids using the water suspension of Fe_3O_4@TiO_2 nanocomposites (containing 1% TFA). Note that the deproteinization problem was observed when methanol was used for extraction instead of water. Therefore, the water suspension was used in the reported experiments for phospholipid extraction in order to prevent the possible effects of plasma deproteinization on the extraction efficiency. After the separation of Fe_3O_4@TiO_2 nanocomposites from the sample matrix, the Fe_3O_4@TiO_2 nanocomposites were rinsed with alkaline extraction solution (1 μL of methanol containing 1.5% NH_4OH (w/w), pH ≈ 9). This allowed the efficient desorption of phospholipids.

To test-proof the performance of d-SPME–iEESI-MS, an aliquot of 0.5 μL of human blood plasma sample from a healthy volunteer was analyzed. Abundant phospholipids such as LysoPC(16:0) (*m/z* 496.34008), PC(34:2) (*m/z* 758.57093), PC(34:1) (*m/z* 760.58557), PC(36:4) (*m/z* 782.56982), PC(36:3) (*m/z* 784.58588), PC(36:2) (*m/z* 786.60110), PC(36:1) (*m/z* 788.61321), PC(38:4) (*m/z* 810.60172), *etc.* were detected in the plasma sample (Fig. 2). Other low abundant mass peaks observed in mass spectra, such as *m/z* 874.78641 and *m/z* 898.78681, were assigned to ammonium adducted triglycerides

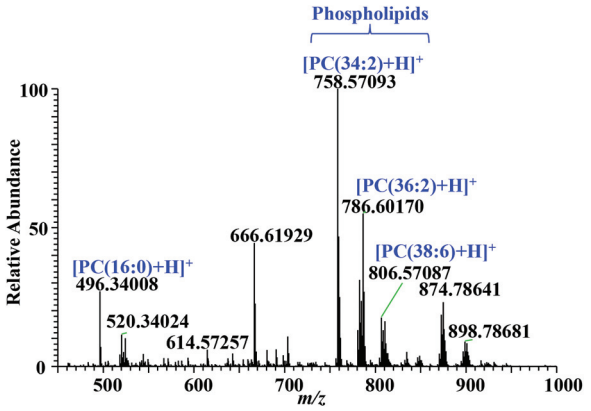

Fig. 2 d-SPME–iEESI-MS of the human blood plasma sample from a healthy volunteer.

(TG) of $[TG(52:3) + NH_4]^+$ and $[TG(54:5) + NH_4]^+$, respectively. The observation of low-abundance triglycerides may be due to the physical adsorption of some triglyceride residues from the blood plasma on the surface of the glass capillary during the sampling process. The identification of PE and SM was based on the results of tandem HCD MS/MS analysis. In HCD, protonated SM species readily yield a protonated phosphocholine head group moiety at *m/z* 184, and protonated PE species yield an abundant characteristic fragment ion of the PE polar head group ($[M + H - 141]^+$) with the neutral loss of phosphoethanolamines (144 Da), which is in agreement with previous reports.[70] The total list of assigned signals is summarized in Table S2, ESI.† Note that only the most abundant out of *ca.* 90 identified phospholipid signals are labelled in Fig. 2 due to space constraints. In our proof-of-principle study the phospholipids were tentatively assigned based on high resolution MS data (with tight mass err within 5 ppm), HCD experiments, measurement of authentic compounds, and earlier literature reports as well as searching across the Human Metabolome Database (http://www.hmdb.ca). Note that the confidence of chemical identification of different classes of phospholipids could be further increased by using the complementary negative ion detection combined with the neutral loss scan and precursor ion scan methods.[31,70] Unfortunately, the neutral loss scan and precursor ion scan methods are not directly available on our hi-res instrument. However, these methods are recommended for more confident chemical identification in the follow-up studies. For reference, the same blood plasma sample was independently analyzed by traditional liquid–liquid extraction combined with ESI-MS (LLE-ESI-MS) and d-SPME–iEESI-MS approaches. Fig. S3, ESI† shows the MS profiles of phospholipids obtained by these two approaches. Most notably, the major phospholipids such as lysoPC(16:0), PC (34:2), and PC(36:4) were observed as predominant ions in the mass spectra obtained by both the methods. However, in LLE-ESI-MS the major phospholipids were mainly observed as sodium adducts ($[M + Na]^+$), whereas in d-SPME–iEESI-MS the major phospholipids were mainly observed in the protonated form ($[M + H]^+$). This observation suggests that in d-SPME–

iEESI-MS inorganic salts (*e.g.*, Na^+ and K^+) are efficiently removed from the sample by sampling and purification processes. In d-SPME–iEESI-MS the spectrum of blood plasma is dominated by phospholipid signals. In contrast, the spectrum of blood plasma obtained by direct nanoESI-MS shows many abundant signals that could not be identified as phospholipids and therefore belong to other molecular types (Fig. S4, ESI†). This comparison indicates the high selectivity of d-SPME–iEESI-MS towards phospholipids. This is consistent with the results of our recent study in which we demonstrated that in acidic solution (1% TFA) phospholipids in blood plasma samples are efficiently adsorbed onto the surface of the TiO_2 material, while other types of molecules such as alkaloids (choline), amino acids (*e.g.*, arginine, lysine, valine, and leucine), sugars (glucose and sucrose), diglycerides, triglycerides, and hemoglobin displayed much lower affinity towards the TiO_2 material.[43] Therefore, we conclude that phospholipids are enriched by the Fe_3O_4@TiO_2 nanocomposites, whereas other nonphosphorylated acidic substances, including inorganic salts, alkaloids, amino acids, sugars, diglycerides, triglycerides, and blood proteins, are largely removed. Note that the analytical performance of our method is expected to be largely retained even if the Fe_3O_4@TiO_2 nanocomposite materials were recycled after each test, as long as the nanomaterials have been carefully washed with the elution solution. However, in the present study, fresh Fe_3O_4@TiO_2 nanocomposite materials were used for each experiment. We found this mode of analysis easier and more robust, particularly given the very low consumption of Fe_3O_4@TiO_2 nanocomposites per run (40 μg), and the low cost and simplicity of nanomaterial synthesis.

3.2 Optimization of the experimental conditions

To improve the analytical performance of d-SPME–iEESI-MS, the experimental conditions, including the ammonia concentration in the desorption solution, the proportion of TFA, and the amount of magnetic nanocomposites used for d-SPME, were optimized. As a proof of concept, phosphate-buffered saline (PBS) was analyzed for the optimization process. Note that PBS is very poorly compatible with traditional ESI-MS and *n*ESI-MS approaches due to the nonvolatility of its components. Spiked LysoPC(16:0) (5 μg L^{-1}) in PBS solution was successfully detected as a protonated ion of *m*/*z* 496.3, which yielded characteristic fragment ions including *m*/*z* 104.1, *m*/*z* 125.0, *m*/*z* 184.1, and *m*/*z* 478.3 under HCD conditions (Fig. S5, ESI†). The dominated fragment ion at *m*/*z* 184.1 belongs to the protonated PC head group ($[C_5H_{14}NO_4P + H]^+$) which is in consistent with the literature.[33] Thus, the signal intensity of the ion at *m*/*z* 184.1 was selected as an analytical indicator to optimize the experimental conditions. As a result, the elution solution of methanol containing 1.5% proportion of ammonia (w/w) was found to be superior to other concentration ratios (Fig. S6a, ESI†), and the TFA concentration in the Fe_3O_4@TiO_2 nanocomposite solution was optimized to 1.5% proportion (Fig. S6b, ESI†). To ensure that the phospholipids in the sample matrix were extracted completely, 10 μL of Fe_3O_4@TiO_2 magnetic nanoparticle suspension containing different amounts of Fe_3O_4@TiO_2 nanocomposite was used for d-SPME–iEESI-MS analysis. The signal intensity of the ion at *m*/*z* 184 was increased by increasing the amount of Fe_3O_4@TiO_2 nanocomposite from 5 μg to 40 μg. However, the signal intensities of the ion at *m*/*z* 184.1 were almost unchanged when the Fe_3O_4@TiO_2 magnetic nanoparticle amount was increased to 60 μg (Fig. S6c, ESI†). Therefore, the Fe_3O_4@TiO_2 nanocomposite amount of 40 μg was adopted in our study. In this study, a fixed volume of elution solution was used to avoid excess dilution of the target phospholipids. 1 μL volume of the elution solvent was used for blood plasma samples. A 0.5 μL elution volume was used for single-cell samples. Note that the larger is the number of magnetic particles the higher is the required volume of elution solvent. Another phospholipid standard of PC(16:0/18:1) was also studied to conform with the established method. Spiked PC (16:0/18:1) (5 μg L^{-1}) in PBS solution was observed as a protonated ion at *m*/*z* 760.6. In HCD the signal at *m*/*z* 760.6 yielded the fragment ions at *m*/*z* 125.0 ($[C_2H_5O_4P + H]^+$) and *m*/*z* 184.1 ($[C_5H_{14}NO_4P + H]^+$) (Fig. S7, ESI†). Furthermore, the usability of negative ion mode detection for MS/MS analysis of phospholipids in our study is demonstrated for PS(18:1/18:1) and PE(18:2/18:0) (Fig. S8, ESI†).

3.3 Analysis of plasma from ovarian cancer patients

Plasma lipidomics is of vital diagnostic potential for a variety of diseases.[5,10,13] Here d-SPME–iEESI-MS was used for rapid scanning of phospholipids in plasma samples donated by ovarian cancer patients and healthy volunteers. Fig. 3 shows typical d-SPME–iEESI-MS fingerprints obtained from the blood plasma samples of ovarian cancer patients and healthy volunteers. The relative abundance of specific phospholipids such as PC(36:4) (*m*/*z* 782.56982), PC(36:2) (*m*/*z* 786.60110), PC(38:6) (*m*/*z* 806.57086), and PC(38:4) (*m*/*z* 810.60172) was notably different between the ovarian cancer patients and

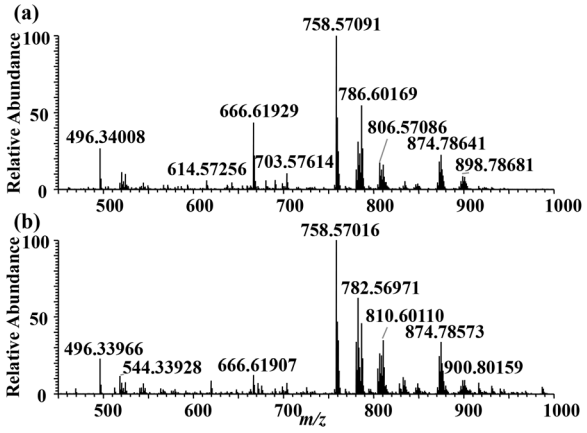

Fig. 3 d-SPME–iEESI-MS analysis of human blood plasma samples donated by healthy volunteers and ovarian cancer patients. (a) Mass spectra obtained from healthy volunteers, (b) mass spectra obtained from patients with ovarian cancer.

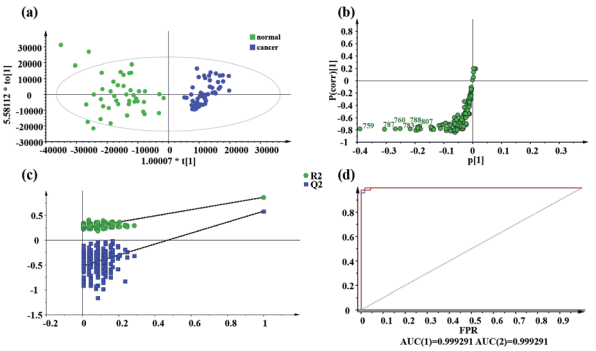

Fig. 4 Differentiation of human blood plasma samples from the patients with ovarian cancer and healthy controls based on OPLS-DA analysis. (a) OPLS-DA score plot of MS data collected from normal blood samples (green) and ovarian cancer blood samples (blue), (b) the S-plot loading plot of the MS data, (c) permutation test result of the OPLS-DA model, (d) ROC plot of the OPLS-DA model.

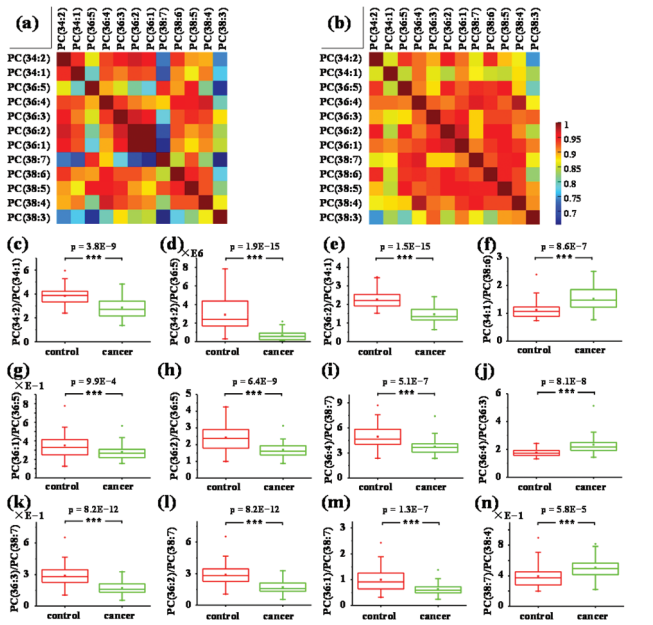

Fig. 5 Correlation among 12 kinds of phospholipids (VIP > 1) and the MS signal intensity ratio for some phospholipids that show significant variation between the healthy controls and ovarian cancer patients. (a) Ovarian cancer patients, (b) healthy controls, (c) signal intensity ratio of PC(34:2) to PC(34:1), (d) signal intensity ratio of PC(34:2) to PC(36:5), (e) signal intensity ratio of PC(36:2) to PC(34:1), (f) signal intensity ratio of PC(34:1) to PC(38:6), (g) signal intensity ratio of PC(36:1) to PC(36:5), (h) signal intensity ratio of PC(36:2) to PC(36:5), (i) signal intensity ratio of PC(36:4) to PC(38:7), (j) signal intensity ratio of PC(36:4) to PC(36:3), (k) signal intensity ratio of PC(36:3) to PC(38:7), (l) signal intensity ratio of PC(36:2) to PC(38:7), (m) signal intensity ratio of PC(36:1) to PC(38:7), and (n) signal intensity ratio of PC(38:7) to PC(38:4). ***denotes P < 0.001, Student's t-test.

healthy controls. Full scan mass fingerprints of a total of 108 human blood plasma samples (including 60 plasma samples of ovarian cancer and 48 healthy control samples) were recorded for statistical analysis based on OPLS-DA analysis. Differences between those two group specimens were visualized by the OPLS-DA score plot (Fig. 4a), in which the healthy controls and patients with ovarian cancer were obviously separated from each other. This result indicated that the molecular differences in plasma phospholipids between the two sample groups were successfully recognized by d-SPME–iEESI-MS.

The S-plot and the variable influence on projection (VIP) value list reveal phospholipids such as PC(34:2) (m/z 758.57093), PC(36:2) (m/z 786.60110), SM(38:1) (m/z 759.63780), PC(36:4) (m/z 782.56982), SM(40:1) (m/z 787.66878), PC(38:6) (m/z 806.57047), PC(36:3) (m/z 784.58588), PC(38:4) (m/z 810.60172), PC(34:1) (m/z 760.58557), PC(36:1) (m/z 788.61321), *etc.* notably contributed to the differentiation of the two kinds of plasma samples (Fig. 4b and Table S3, ESI†), which suggests that the corresponding phospholipids with higher VIP value (VIP > 1) may act as potential diagnostic biomarkers of ovarian cancer. A permutation test with 200 iterations was performed to validate the OPLS-DA model, and the result showed that the model was not overfitted, as the true-class Q^2 and R^2 values to the right were significantly higher than the corresponding permutated values to the left (Fig. 4c). The receiver operating characteristic (ROC) analysis was also performed to evaluate the reliability of the model, and the ROC curve illustrates the combined discriminatory performance of a group with area under the curve (AUC) >0.99 (Fig. 4d). Thus, the OPLS-DA model was valid in the differentiation of ovarian cancer patients and healthy controls. Indeed, the study on a larger group of samples is needed to validate the method for the clinical diagnosis of ovarian cancer. This work is currently ongoing in our laboratory.

To further investigate the differences in the phospholipid composition between the ovarian cancer patients and the healthy controls, 12 kinds of phospholipids with their corresponding VIP > 1 were selected for correlation analysis. As shown in Fig. 5, their correlation associations in the ovarian cancer patients and healthy controls were notably different from each other, indicating that the metabolic changes of multi-type phospholipids happened in the pathological process of ovarian cancer. Particularly pronounced variations (P < 0.001, Student's t-test) were found in the ratios of PC (34:2)/PC(34:1), PC(34:2)/PC(36:5), PC(36:2)/PC(34:1), PC(34:1)/PC(38:6), PC(36:1)/PC(36:5), PC(36:2)/PC(36:5), PC(36:4)/PC (38:7), PC(36:4)/PC(36:3), PC(36:3)/PC(38:7), PC(36:2)/PC(38:7), PC(36:1)/PC(38:7), and PC(38:7)/PC(38:4) (Fig. 5). The signal ratios of PC(34:2)/PC(34:1), PC(34:2)/PC(36:5), PC(36:2)/PC (34:1), PC(36:1)/PC(36:5), PC(36:2)/PC(36:5), PC(36:4)/PC(38:7), PC(36:3)/PC(38:7), PC(36:2)/PC(38:7), and PC(36:1)/PC(38:7) were significantly lower in ovarian cancer patients compared to the controls, while increased unsaturation of phosphatidylcholines of PC(36:1), PC(36:4) and PC(38:7) were found in patients compared to PC(36:5), PC(36:3) and PC(38:4) in the controls(Fig. 5). Previous studies have shown that the dysregulation of phosphatidylcholines may change the microenvironment of cancer cells, thus affecting the membrane fluidity and membrane structure.[71,72] These results indicate that phos-

pholipids which are correlated with cell malignancy can be helpful for the recognition of ovarian cancer.

3.4 Analysis of plasma from pancreatic cancer patients

Human blood plasma samples from pancreatic cancer patients were also tested by the proposed method. Here the plasma specimens contain 28 samples from pancreatic cancer patients and 23 samples from healthy volunteers. The representative blood plasma mass spectra of pancreatic cancer patients and healthy controls are shown in Fig. S9, ESI.† To visualize the phenotype differences in the plasma phospholipids between the patients with pancreatic cancer and the healthy controls, the obtained fingerprints of the total 51 blood plasma samples were subjected to OPLS-DA analysis. The score plot shows that the pancreatic cancer patients and healthy controls were successfully discriminated from each other (Fig. S9a, ESI†). The differentiation model was validated by 200 permutation tests and ROC analysis, yielding satisfactory Q^2, R^2, and AUC values (Fig. S10b and c, ESI†), which indicate that a robust model is built to describe the differentiation of pancreatic cancer. The S-plot shows that phospholipids such as PC(32:1) (732.55507), PC(34:2) (*m*/*z* 758.57093), PC(34:1) (*m*/*z* 760.58557), PC(36:4) (*m*/*z* 782.56982), PC(36:2) (*m*/*z* 786.60110), *etc*. notably contributed to the differentiation of the two kinds of plasma samples (Fig. S10d and Table S4, ESI†). Thus, the changes in the phospholipid composition associated with pancreatic cancer can be visualized by d-SPME–iEESI-MS combined with OPLS-DA analysis.

The correlation of 14 phospholipids with their corresponding VIP > 1 are shown in Fig. S11, ESI.† The correlation of these 14 phospholipids in the pancreatic cancer patients and healthy controls was different between each other. Similarly, the correlation of the major phospholipids in the ovarian cancer patients and healthy controls also showed a significant difference between each other. These results further indicate that the dysregulation of phospholipids in cancer may be associated with the alteration of the phospholipid composition. Interestingly, phospholipids with VIP > 1, which had the strongest contribution to the recognition of cancer specimens, including PC(34:2), PC(34:1), PC(36:5), PC (36:4), PC(36:3), PC(36:2), PC(38:6), PC(38:5), PC(38:4), and PC(38:3), were found in both ovarian cancer and pancreatic cancer samples, and phospholipids PC(36:1) and PC(38:7) were mostly correlated with ovarian cancer, while PC(32:1), PC(34:3), PC(34:0), and PC(36:0) were mostly correlated with pancreatic cancer (Tables S3 and S4, ESI†). The differences in these phospholipids with VIP > 1 between ovarian cancer and pancreatic cancer may be related to the intrinsic difference of these two kinds of cancers, which potentially provides the possibility for the recognition of different cancers based on the molecular differences in their phospholipid profiles. The study of more cancer species together with larger group of samples is needed to systematically analyze the variation in phospholipid components associated with different cancers. This work is currently ongoing in our laboratory.

3.5 Analysis of single cell samples

In recent years, single-cell metabolic, proteomic, and genomic studies have attracted increasing attention.[15–19] The molecular analysis of a single cell is still a high challenge due to the tiny size of the cell and complexity of the cell chemical matrix. Here, the proposed method was tested for the determination of phospholipids in single human cells. Two kinds of human leukemia cell subpopulations including the single MV4–11 cell (biphenotypic B-myelomonocytic leukemia cells) and single NB4 cell (acute promyelocytic leukemia cell) were analyzed by d-SPME–iEESI-MS. As shown in Fig. 6a, protonated phospholipids such as PC(32:0), PC(34:2), PC(34:1), PC(36:4), PC(36:3), and PC(36:2) were detected from single MV4–11 cell and single NB4 cell. Due to the tiny amount of the total chemical material in a single cell, the signal duration of each sample was only *ca.* 10 s and the phospholipid signals were of relatively low abundance in the mass spectra (Fig. 6a and b). However, despite the low intensity, the phospholipid signals could be clearly distinguished from the EIC of target phospholipids (Fig. S12, ESI†), which confirms the determination of phospholipids in the single-cell samples. The mass spectra fingerprints of single MV4–11 cell and single NB4 cell were further processed by OPLS-DA analysis. The OPLS-DA result of the two kinds of cell types is shown in Fig. 6c. The heterogeneity between these two cell subpopulations was evidently revealed through OPLS-DA, and the two kinds of cell subpopulations were successfully classified into separate colonies. The results of the permu-

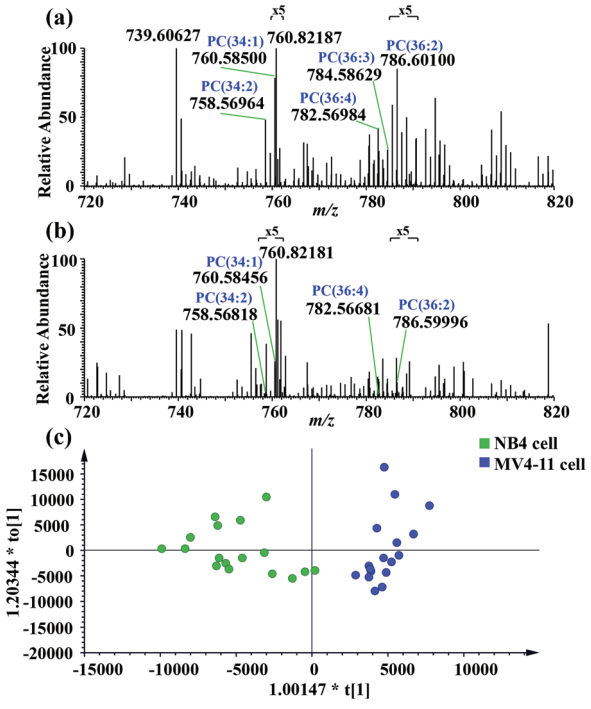

Fig. 6 d-SPME–iEESI-MS analysis of single-cell subpopulations. (a) Mass spectra obtained from a single MV4–11 cell, (b) mass spectra obtained from a single NB4 cell, and (c) OPLS-DA score plot of the two cell types.

tation test performed with 200 iterations also indicated the validity of the OPLS-DA model (Fig. S13, ESI†). The results indicate that the developed method can achieve sensitive and selective analysis of phospholipids in single-cells and have the potential for the identification of cell populations. Note that the two types of cells used in this study belong to different cancer cells. The comparison of single cancer cells and single healthy cells is an interesting topic for future research.

3.6. Evaluation of signal linearity and LOD

Based on the optimized experimental conditions, the signal response for the determination of phospholipids using d-SPME–iEESI-MS was evaluated. LysoPC(16:0) and PC(16:0/18:1) stock solutions were spiked in PBS to make a series of working solutions in the range of 0.1–300.0 μg L^{-1} for d-SPME–iEESI-MS/MS analysis. The signal response curves of LysoPC(16:0) and PC(16:0/18:1) are shown in Fig. S14, ESI.† Linear R^2 values ≥0.99 were obtained in both cases. The limit of detection (LOD) values of LysoPC(16:0) and PC(16:0/18:1) in PBS samples defined by a signal-to-noise ratio (S/N) of 3 were estimated to be 0.015 μg L^{-1} and 0.013 μg L^{-1}, respectively. The RSD values of six replicates were below 9.1% (n = 6) for the both the compounds (for details see Table S5, ESI†). The analysis of one sample took less than 4 min. Recovery rates at three different spiked concentrations were from 96.3% to 112.9%, with RSDs ≤7.1% (n = 6) for LysoPC(16:0), and from 98.6% to 111.8%, with RSDs ≤6.1% (n = 6) for PC(16:0/18:1) (details in Table S5, ESI†). Note that the difference in the signal intensity of the ion at m/z 184 of PC(16:0/18:1) and LysoPC(16:0) in the HCD experiments is most probably due to the difference in the fatty-acyl substituents and molecular weights of these two compounds, as indicated by earlier research.[70] Following the approach by Bjarnason,[73] the extraction efficiency (E, %) of a certain phospholipid type was evaluated as the ratio of its mass after the d-SPME process to its mass in the initial sample solution. The extraction efficiencies of LysoPC(16:0) (250 μg L^{-1}) and PC(16:0/18:1) (200 μg L^{-1}) from PBS solution samples were evaluated to be 92.5 ± 6.1% (n = 4) and 95.5 ± 6.1% (n = 4), respectively. Furthermore, the detection of other types of standard phospholipids such as PS (18:1/18:1), PE(18:2/18:0) and SM(d18:1/16:0) was also demonstrated using the present method (Fig. S8, ESI†). The LODs for PS(18:1/18:1), PE(18:2/18:0), and SM(d18:1/16:0) were estimated to be 0.035 μg L^{-1}, 0.019 μg L^{-1}, and 0.015 μg L^{-1}, respectively. In comparison with the results of detection of phospholipids based on TiO_2 nanowires-iEESI-MS in our previous research,[43] the proposed method offers *ca.* two-times higher chemical sensitivity, which is probably owing to a considerably higher active surface area of the adsorbent in d-SPME compared to the conventional mode of extraction.[34,48] Another important advantage of the proposed method is its suitability for the analysis of microvolume samples, which opens new possibilities for single-cell analysis and non-invasive clinical diagnostics. The experimental results indicate that the proposed method is potentially useful for rapid quantitative analysis of phospholipids in biofluid samples. Note that for the quantitative analysis of phospholipids by our method internal standards such as isotopically-labeled phospholipids could be spiked into the samples for compensation of analytical errors associated with possible signal instability and matrix effects.[31]

4. Conclusions

To conclude, the rapid and selective determination of phospholipids in human blood plasma samples and single cells was achieved by dispersed solid phase microextraction with Fe_3O_4@TiO_2 nanoparticles coupled with internal extractive electrospray ionization mass spectrometry (d-SPME–iEESI-MS). Efficient extraction and desorption of phospholipids based on dispersed Fe_3O_4@TiO_2 nanocomposites was achieved inside a capillary with very low consumption of both the sample solution (≤0.5 μL per test) and nanomaterial (40 μg per test). Phospholipids in the blood plasma samples donated from ovarian cancer patients, pancreatic cancer patients, and healthy volunteers were successfully detected by the proposed method in combination with a statistical analysis method. The versatility of the proposed method was also further demonstrated by the analysis of phospholipids in single cells, thus providing a method for profiling the phospholipid heterogeneity of cells and cell classification. Note that, based on the facile method, other magnetic nanocomposite particles could also be employed in d-SPME–iEESI-MS for the determination of other target chemicals, which could further extend the application of the proposed method. The major advantages of the combination d-SPME with iEESI-MS include high sensitivity, high specificity, low sample consumption, high speed and good suitability for high-throughput analysis.

Conflicts of interest

There are no conflicts to declare.

Acknowledgements

The work was supported by the National Natural Science Foundation of China (No. 21765001 and 21705017), the Natural Science Foundation of Jiangxi Province (No. 20165BCB19013), and the National Key R&D Program of China (No. 2018YFA0106920); K.C. acknowledges financial support from the Russian Science Foundation (Agreement #20-65-46014).

References

1 F. H. Westheimer, *Science*, 1987, **235**, 1173–1178.
2 Y. Nishizuka, *Science*, 1992, **258**, 607–614.
3 M. Holcapek, G. Liebisch and K. Ekroos, *Anal. Chem.*, 2018, **90**, 4249–4257.

4 M. A. Lemmon, *Nat. Rev. Mol. Cell Biol.*, 2008, **9**, 99–111.
5 T. Balla, *Physiol. Rev.*, 2013, **93**, 1019–1137.
6 R. Bandu, H. J. Mok and K. P. Kim, *Mass Spectrom. Rev.*, 2018, **37**, 107–138.
7 A. Ghosh and K. Nishtala, *Clin. Transl. Med.*, 2017, **6**, 22.
8 J. V. Swinnen, K. Brusselmans and G. Verhoeven, *Curr. Opin. Clin. Nutr.*, 2006, **9**, 358–365.
9 M. Borkman, L. H. Storlien, D. A. Pan, A. B. Jenkins, D. J. Chisholm and L. V. Campbell, *N. Engl. J. Med.*, 1993, **328**, 238–244.
10 M. Mapstone, A. K. Cheema, M. S. Fiandaca, X. Zhong, T. R. Mhyre, L. H. MacArthur, W. J. Hall, S. G. Fisher, D. R. Peterson, J. M. Haley, M. D. Nazar, S. A. Rich, D. J. Berlau, C. B. Peltz, M. T. Tan, C. H. Kawas and H. J. Federoff, *Nat. Med.*, 2014, **20**, 415–418.
11 J. A. Conquer, M. C. Tierney, J. Zecevic, W. J. Bettger and R. H. Fisher, *Lipids*, 2000, **35**, 1305–1312.
12 M. R. Prasad, M. A. Lovell, M. Yatin, H. Dhillon and W. R. Markesbery, *Neurochem. Res.*, 1998, **23**, 81–88.
13 B. G. Nordestgaard, M. J. Chapman, K. Ray, J. Boren, F. Andreotti, G. F. Watts, H. Ginsberg, P. Amarenco, A. Catapano, O. S. Descamps, E. Fisher, P. T. Kovanen, J. A. Kuivenhoven, P. Lesnik, L. Masana, Z. Reiner, M.-R. Taskinen, L. Tokgozoglu and A. Tybjaerg-Hansen, *Eur. Heart J.*, 2010, **31**, 2844–2853.
14 J. F. Oram and J. W. Heinecke, *Physiol. Rev.*, 2005, **85**, 1343–1372.
15 H. Zhu, N. Wang, L. Yao, Q. Chen, R. Zhang, J. Qian, Y. Hou, W. Guo, S. Fan, S. Liu, Q. Zhao, F. Du, X. Zuo, Y. Guo, Y. Xu, J. Li, T. Xue, K. Zhong, X. Song, G. Huang and W. Xiong, *Cell*, 2018, **173**, 1716–1727.
16 A. M. Klein, L. Mazutis, I. Akartuna, N. Tallapragada, A. Veres, V. Li, L. Peshkin, D. A. Weitz and M. W. Kirschner, *Cell*, 2015, **161**, 1187–1201.
17 J. R. Heath, A. Ribas and P. S. Mischel, *Nat. Rev. Drug Discovery*, 2016, **15**, 204–216.
18 W. F. Zhang, N. Li, L. Lin, Q. S. Huang, K. Uchiyama and J. M. Lin, *Small*, 2020, **16**, 1903402.
19 Q. S. Huang, S. F. Mao, M. Khan, W. W. Li, Q. Zhang and J. M. Lin, *Chem. Sci.*, 2020, **11**, 253–256.
20 M. R. Wenk, *Cell*, 2010, **143**, 888–895.
21 P. Liu, Q. S. Huang, M. Khan, N. Xu, H. R. Yao and J. M. Lin, *Anal. Chem.*, 2020, **92**, 7900–7906.
22 G. K. Ramachandran, W. P. Yong and C. H. Yeow, *PLoS One*, 2016, **11**, e0162222.
23 S. Kaffarnik, I. Ehlers, G. Grobner, J. Schleucher and W. Vetter, *J. Agric. Food Chem.*, 2013, **61**, 7061–7069.
24 N. Jin, K. T. Semple, L. Jiang, C. Luo, D. Zhang and F. L. Martin, *Analyst*, 2018, **143**, 768–776.
25 C. Woess, S. H. Unterberger, C. Roider, M. Ritsch-Marte, N. Pemberger, J. Cemper-Kiesslich, P. Hatzer-Grubwieser, W. Parson and J. D. Pallua, *PLoS One*, 2017, **12**, e0174552.
26 K. Czamara, K. Majzner, M. Z. Pacia, K. Kochan, A. Kaczor and M. Baranska, *J. Raman Spectrosc.*, 2015, **46**, 4–20.
27 S. Feng, R. Chen, J. Lin, J. Pan, G. Chen, Y. Li, M. Cheng, Z. Huang, J. Chen and H. Zeng, *Biosens. Bioelectron.*, 2010, **25**, 2414–2419.
28 Y. H. Rustam and G. E. Reid, *Anal. Chem.*, 2018, **90**, 374–397.
29 R. C. Murphy, *TrAC, Trends Anal. Chem.*, 2018, **107**, 91–98.
30 F.-F. Hsu, *Anal. Bioanal. Chem.*, 2018, **410**, 6387–6409.
31 T. Cajka and O. Fiehn, *TrAC, Trends Anal. Chem.*, 2014, **61**, 192–206.
32 X. Han, K. Yang and R. W. Gross, *Mass Spectrom. Rev.*, 2012, **31**, 134–178.
33 X. L. Han and R. W. Gross, *Mass Spectrom. Rev.*, 2005, **24**, 367–412.
34 N. Reyes-Garces, E. Gionfriddo, G. A. Gmez-Rios, M. N. Alam, E. Boyaci, B. Bojko, V. Singh, J. Grandy and J. Pawliszyn, *Anal. Chem.*, 2018, **90**, 302–360.
35 H. Kataoka, H. L. Lord and J. Pawliszyn, *J. Chromatogr. A*, 2000, **880**, 35–62.
36 H. Lord and J. Pawliszyn, *J. Chromatogr. A*, 2000, **885**, 153–193.
37 L. Fang, J. Deng, Y. Yang, X. Wang, B. Chen, H. Liu, H. Zhou, G. Ouyang and T. Luan, *TrAC, Trends Anal. Chem.*, 2016, **85**, 61–72.
38 J. Deng, Y. Yang, X. Wang and T. Luan, *TrAC, Trends Anal. Chem.*, 2014, **55**, 55–67.
39 G. A. Gomez-Rios and J. Pawliszyn, *Angew. Chem., Int. Ed.*, 2014, **53**, 14503–14507.
40 G. A. Gomez-Rios, E. Gionfriddo, J. Poole and J. Pawliszyn, *Anal. Chem.*, 2017, **89**, 7240–7248.
41 J. Deng, W. Li, Q. Yang, Y. Liu, L. Fang, Y. Guo, P. Guo, L. Lin, Y. Yang and T. Luan, *Anal. Chem.*, 2018, **90**, 6936–6944.
42 Z. Zhang, W. Xu, N. E. Manicke, R. G. Cooks and Z. Ouyang, *Anal. Chem.*, 2012, **84**, 931–938.
43 H. Zhang, K. Chingin, J. Li, H. Lu, K. Huang and H. Chen, *Anal. Chem.*, 2018, **90**, 12101–12107.
44 W. Gao, Y. Tian, H. Liu, Y. Cai, A. Liu, Y.-L. Yu, Z. Zhao and G. Jiang, *Anal. Chem.*, 2018, **91**, 772–775.
45 X. Gong, Y. Zhao, S. Cai, S. Fu, C. Yang, S. Zhang and X. Zhang, *Anal. Chem.*, 2014, **86**, 3809–3816.
46 C.-H. Wang, H. Su, J.-H. Chou, M.-Z. Huang, H.-J. Lin and J. Shiea, *Anal. Chim. Acta*, 2018, **1021**, 60–68.
47 X. Wang, X. Li, Z. Li, Y. Zhang, Y. Bai and H. Liu, *Anal. Chem.*, 2014, **86**, 4739–4747.
48 A. Mehdinia and M. O. Aziz-Zanjani, *TrAC, Trends Anal. Chem.*, 2013, **51**, 13–22.
49 H. Y. Lu, H. Zhang, K. Chingin, Y. P. Wei, J. Q. Xu, M. F. Ke, K. K. Huang, S. H. Feng and H. W. Chen, *Anal. Chem.*, 2019, **91**, 10532–10540.
50 H. Zhang, K. Chingin, L. Zhu and H. W. Chen, *Anal. Chem.*, 2015, **87**, 2878–2883.
51 H. Zhang, L. Zhu, L. P. Luo, N. N. Wang, K. Chingin, X. L. Guo and H. W. Chen, *J. Agric. Food Chem.*, 2013, **61**, 10691–10698.
52 H. Zhang, H. Gu, F. Yan, N. Wang, Y. Wei, J. Xu and H. Chen, *Sci. Rep.*, 2013, **3**, 2495.
53 J. Han, W. Liu, R. Su, L. X. Zhu, D. B. Wu, J. Q. Xu, A. Y. Liu, H. Zhan, W. Kou, X. P. Zhang and S. P. Yang, *Anal. Bioanal. Chem.*, 2019, **411**, 3281–3290.

54 H. Zhang, H. Lu, H. Huang, J. Liu, X. Fang, B.-F. Yuan, Y.-Q. Feng and H. Chen, *Anal. Chim. Acta*, 2016, **926**, 72–78.
55 H. Zhang, W. Kou, A. S. Bibi, Q. Jia, R. Su, H. W. Chen and K. K. Huang, *Sci. Rep.*, 2017, **7**, 14714.
56 A. Y. Liu, W. Kou, H. Zhang, J. Q. Xu, L. X. Zhu, S. L. Kuang, K. K. Huang, H. W. Chen and Q. Jia, *Anal. Chem.*, 2020, **92**, 4137–4145.
57 A. Leitner, *TrAC, Trends Anal. Chem.*, 2010, **29**, 177–185.
58 F. Y. Gao, F. L. Jiao, C. S. Xia, Y. Zhao, W. T. Ying, Y. P. Xie, X. Y. Guan, M. Tao, Y. J. Zhang, W. J. Qin and X. H. Qian, *Chem. Sci.*, 2019, **10**, 1579–1588.
59 Y. R. Huang, Q. X. Zhou, J. P. Xiao and G. H. Xie, *J. Sep. Sci.*, 2010, **33**, 2184–2190.
60 M. D. E. Goodyear, K. Krleza-Jeric and T. Lernmens, *Br. Med. J.*, 2007, **335**, 624–625.
61 H. T. Zhang, J. E. Kacharmina, K. Miyashiro, M. I. Greene and J. Eberwine, *Proc. Natl. Acad. Sci. U. S. A.*, 2001, **98**, 5497–5502.
62 B. G. Lambrus, T. C. Moyer and A. J. Holland, in *Mitosis and Meiosis, Pt A*, ed. H. Maiato and M. Schuh, Elsevier Academic Press Inc, San Diego, 2018, vol. 144, pp. 107–135.
63 S. Guo, Y. Wang, D. Zhou and Z. Li, *Sci. Rep.*, 2014, **4**, 5959.
64 J. Liu, R. G. Cooks and Z. Ouyang, *Anal. Chem.*, 2011, **83**, 9221–9225.
65 N. Yu, S. Wei, M. Li, J. Yang, K. Li, L. Jin, Y. Xie, J. P. Giesy, X. Zhang and H. Yu, *Sci. Rep.*, 2016, **6**, 23963.
66 J. Zhang, J. Xu, Y. Ouyang, J. Liu, H. Lu, D. Yu, J. Peng, J. Xiong, H. Chen and Y. Wei, *Sci. Rep.*, 2017, **7**, 3738.
67 A. Gonzalvez, B. Preinerstorfer and W. Lindner, *Anal. Bioanal. Chem.*, 2010, **396**, 2965–2975.
68 Q. Shen and H.-Y. Cheung, *J. Agric. Food Chem.*, 2014, **62**, 8944–8951.
69 P. A. Connor and A. J. McQuillan, *Langmuir*, 1999, **15**, 2916–2921.
70 M. Pulfer and R. C. Murphy, *Mass Spectrom. Rev.*, 2003, **22**, 332–364.
71 L. S. Eberlin, I. Norton, A. L. Dill, A. J. Golby, K. L. Ligon, S. Santagata, R. G. Cooks and N. Y. R. Agar, *Cancer Res.*, 2012, **72**, 645–654.
72 J. L. Spratlin, N. J. Serkova and S. G. Eckhardt, *Clin. Cancer Res.*, 2009, **15**, 431–440.
73 B. Bjarnason, L. Chimuka and O. Ramstrom, *Anal. Chem.*, 1999, **71**, 2152–2156.